

DOI: 10.1002/adhm. 201300075

Article type: Communication

Title: Inhibition of Cancer Cell Migration by Multiwalled Carbon Nanotubes

*Lorena García-Hevia, Rafael Valiente, José L. Fernández-Luna, Emanuel Flahaut, Lidia Rodríguez-Fernández, Juan C. Villegas, Jesús González, Mónica L. Fanarraga**

L. G-H. Departamento de Biología Molecular, Universidad de Cantabria-IDIVAL, 39011, Santander. Spain.

R.V. Departamento de Física Aplicada, Facultad de Ciencias, Universidad de Cantabria-IDIVAL, 39005 Santander, Spain

J. L. F-L. Hospital Valdecilla-IDIVAL, 39011, Santander, Spain

E. F. CNRS, Université de Toulouse, Institut Carnot CIRIMAT, F-31062 Toulouse, France

L. R-F. SERMET, Universidad de Cantabria, 39005, Santander, Spain

J. C. V. Departamento de Anatomía y Biología Celular, Universidad de Cantabria-IDIVAL, 39011, Santander. Spain.

J. G. MALTA-Consolider Team, CITIMAC, Facultad de Ciencias, Universidad de Cantabria-IDIVAL, 39005 Santander, Spain

* M.L. F. Departamento de Biología Molecular, Universidad de Cantabria-IDIVAL, 39011, Santander. Spain.

Email: fanarrag@unican.es

Keywords: cytoskeleton, biomechanics, tubulin polymer, cancer, metastasis

Finding ways to control cancer at the primary site means the difference between life and death.

Localized tumors can be eliminated by surgery and radiation therapy, and as a general rule do not represent a life-threatening problem. However, when cancer spreads to other tissues it becomes an incurable condition where treatments can only delay the progression of the disease and prolong survival.

Carbon nanotubes (CNTs) represent a highly versatile heterogeneous family of nanomaterials that display interesting physico-chemical properties.^[1] These nanomaterials are well-known to interact with the biological matter, penetrating inside tissues and cells,^[2,3] leading to a plethora of side effects in living organisms.^[4-7] *In vitro*, CNTs can be actively captured by most cells.^[2-3] Once inside the cells, CNTs intermingle with many subcellular structures also at nano-scale, mostly filaments such as DNA,^[8] actin^[9,10] or microtubules.^[5,11] In particular, multiwalled carbon nanotubes (MWCNTs) have been shown to contact cell surface receptors,^[2] translocate across cell membranes *via* the endocytic pathway in both, phagocytic and non-phagocytic cells,^[2,3] and interfere with the microtubule function triggering anti-proliferative and pro-apoptotic effects.^[5,10,11]

MWCNTs display interesting biomimetic properties with microtubules.^[11-13] These cytoskeletal elements are intracellular protein nanotubes that result from the self-association of tubulin into 4 nm polymers, known as protofilaments.^[14] Tubulin protofilaments are organized into a circle assembling a 25 nm diameter tube, the microtubule (**Figure S1**). Thus, MWCNTs and microtubules are both 1D hollow nanofilaments with a similar length-to-diameter ratio, resiliency, self-assembly properties and a comparable surface reactivity^[12] that favors their association into bio-synthetic polymers both, *in vitro*^[13] and *in vivo*.^[11] There is however, a big difference between these two nanofilaments that has chief biotechnological implications. While CNTs are very stable filaments, microtubules are highly dynamic polymers that stochastically switch between phases of polymerization-depolymerization on

the time scale of seconds both, *in vitro* and *in vivo*.^[16,17] During mitosis, the microtubule dynamic behavior increases 20- to 100-fold to assemble the so-called “mitotic spindle”, a microtubule-based structure responsible for the balanced segregation of the chromosomes between the daughter cells.^[17] Some of the most widely used anti-neoplastic drugs such as paclitaxel (taxol®) and their derivatives are microtubule-binding chemicals that behave as spindle poisons, inhibiting cell proliferation, leading to mitotic arrest and cell death.^[16-19]

MWCNTs interact tubulin intracellularly assembling biosynthetic filaments.^[11] These hybrid microtubules display a significantly enhanced stability compared to the standard tubulin polymers that favors non-centrosomal cytoplasmic microtubule nucleation. As the word “*centro-some*” means, this structure is a key organizer of the microtubule cytoskeleton in the cell, participating in all cellular activities including cell division and migration. CNT-triggered centrosomal abnormalities are well documented in the literature. These include aberrant mitotic spindle assemblies, chromosomal malsegregation, abnormal interphase microtubule arrays and cytotoxicity in general.^[5,11,20] Since centrosomal positioning is a key structure in migrating cells, conferring membrane and cytoskeletal directionality, here we determine if MWCNTs have the intrinsic ability to hinder cancer cell spreading and discuss the molecular mechanics behind this effect.

For the study we first determined the position and trajectory of the centrosome in migrating HeLa cells treated with MWCNTs. As a rule of thumb, migrating cells display a polarized morphology^[21] determined by the so-called, nuclear-centrosomal axis (Figure 1A). This axis, first identified by Van Beneden in the 1880s,^[22] contributes to the asymmetric organization of cell structure during migration, and corresponds to the final direction of the displacement.^[23]

Microtubules, connected to the migrating front of the cell, pull forward the centrosome dragging the nucleus forward, thus redistributing the traction forces generated at the cell's migrating front, to the centrosome, and throughout the cytoplasm to produce an effective net

cell body translation. Accordingly, in cells migrating on 2D substrates, the centrosome is typically positioned between the nucleus and the leading edge, along this axis. To determine the orientation of nuclear-centrosomal axis we performed *time-lapse* video microscopy on live HeLa cells displaying fluorescently labelled centrosomes and nuclei (Experimental section). This allowed comparing this axis with the direction of the cell trajectory in migrating MWCNT-treated cells and untreated controls. As summarized in **Figure 1B**, in frozen live-cell images obtained from **Supporting Video 1-3**, the centrosomes in MWCNT-treated cells displayed a random peri-nuclear location and were aberrantly positioned with respect to the nuclear trajectory. As a result, in MWCNT-treated cells the direction of the cell migration (white arrows) and the nuclear-centrosomal axes (yellow arrows) were not parallel. Conversely, in untreated-control HeLa cells centrosomes were located along the nuclear-centrosomal axis, between the nucleus and the leading edge of the cells, just as described by Van Beneden.

To investigate the consequences of these findings, we calculated the average migration speed of control and MWCNT-treated cells using cell tracking analysis (Experimental section). For the study we investigated various cancer cell lines including (i) HeLa cells, (ii) MCF7 cells, a human breast cancer cell line; (iii) SH-SY5Y cells, a neuroblastoma cell line originally established from a metastatic tumor; (iv) and U87MG cells, a grade IV human glioma cell line. Cells were incubated with 25 µg/ml MWCNTs for 70 h and were *time-lapse* video recorded for 5 h. This MWCNT concentration produced no obvious signs of toxicity but revealed a reduction of more than 40 % in the average speed of HeLa cells treated with MWCNTs. A statistically significant cell speed reduction was also shown for the other two fast-migrating cancer cell lines, SH-SY5Y and U87MG when exposed to MWCNTs (**Table 1, Figure 1C, D**). A possible interference with MWCNTs settled on the growing matrix was also considered. However, under our functionalization conditions MWCNTs precipitation or aggregation on

the growing matrix is never observed. Besides, recent studies have shown that CNTs facilitate cell migration.^[24]

To further demonstrate our hypothesis we decided to replicate this experiment on real tumor cells isolated from surgical specimens. Characteristically, tumor-explant derived cancer cells are much more heterogeneous than most cancer cell line models. We chose glioblastoma multiforme cells (GBM) for the study because these cells typically infiltrate the surrounding brain tissue leading to tumor recurrence after surgery. Glioblastomas are the most common and aggressive primary brain tumor in adults, and have an unfavorable prognosis with a median survival time of less than fifteen months, mostly due to recurrence. For the study we isolated GBM cells from surgical specimens that were fully characterized^[25] before exposure to 25 µg/ml MWCNTs for 70 h. This experiment served to confirm that MWCNTs also triggered a significant anti-migratory effect (18 % speed reduction) in real tumor-derived cells (**Figure 2A, Table 1**).

The presence of intracellular MWCNTs in GBM cells was confirmed using confocal Raman spectroscopy focusing the laser within the cell's cytoplasm. We observed differences in the peak positions in the spectrum of intracellular MWCNTs, slightly shifted to higher wavenumbers (**Figure 2B, inset**), together with a decrease in Raman intensities of the D, G and G' modes (**Figure 2B, Supplementary Table 1**). As it has been previously shown, CNTs exhibit variations in the relative Raman intensities and/or positions for various Raman modes depending on different physical^[26] or chemical^[27,28] environments and according their agglomeration state. In this study, functionalized intracellular MWCNTs display a well pronounced G mode indicative of a significant dispersion. The overall data also indicated that the coating of MWCNTs did not significantly affect the G mode profile, as previously reported for non-covalently-modified SWCNTs dispersed in aqueous solutions containing peptides^[26-32] or proteins.^[33-34] The precise cytoplasmic distribution of the intracellular

MWCNTs was also determined on a single confocal Z plane obtained across the GBM cell cytoplasm using confocal Raman imaging, following the G band at 1586 cm^{-1} (**Figure 2C, D**). This technique revealed how intracellular MWCNTs were localized in small spots throughout the cytoplasm, a distribution coinciding with that previously described in MWCNT-treated cell lines.^[11] These experiments demonstrate how MWCNTs can also translocate inside surgical specimen-derived cancer cells, and how these nanomaterials can also hinder GBM cell spreading.

Finally, we also explored if the observed anti-migratory effect was dose-dependent. For the study we treated all the neural-derived cell lines and the primary GBM cell cultures with 0, 25, 50 and 75 $\mu\text{g/ml}$ of MWCNTs in the growing medium for 70 h. Again, this analysis confirmed a statistically significant speed reduction, of up to 62 %, with dosages of 50 $\mu\text{g/ml}$ (**Supplementary Table 2**). Larger dosages (75 $\mu\text{g/ml}$) triggered a massive cytotoxic effect, suggesting excess MWCNTs probably interfere with some other critical cellular processes leading to cell death.

The interaction of nanomaterials with proteins or lipids, the actual biological building blocks, is still poorly understood as reviewed by Tay and colleagues.^[35] These studies demonstrate that MWCNTs could play a pivotal role in cancer treatment in combination to standard therapies interfering with cancer cell migration. Other nanomaterials such as TiO_2 , SiO_2 , and hydroxyapatite nanoparticles have also been recently shown to interfere with cell migration damaging the microtubule network.^[36] Our work demonstrates that MWCNTs could play a pivotal role in cancer treatment in combination to standard therapies interfering with cancer cell migration. We have previously documented the molecular interaction of MWCNTs with tubulin intracellularly,^[11] and how the biomimetic properties of MWCNTs obstruct microtubule function during mitosis behaving as spindle poisons, same as traditional microtubule-binding drugs such as taxol®. Remarkably, the interaction of MWCNTs with the

1 microtubule is not site-specific. Instead MWCNTs appear to interact along the protofilament
2 surface,^[37] and this fact has two major advantages. First, MWCNTs do not require a specific
3 binding site in the tubulin molecule subject of mutations. And second, the MWCNTs
4 interaction with microtubules permits other microtubule-binding drugs to interact with their
5 structural pocket in the tubulin molecule. Here we show how, in addition to the anti-
6 proliferative effect of MWCNTs, these nanomaterials also display important anti-migratory
7 effects in cancer cells. This new intrinsic feature of MWCNTs could significantly boost the
8 mechanism of action of traditional microtubule-binding cytotoxic chemotherapies^[16-18] and
9 thus might serve to bypass some of the drug-resistance mechanisms in cancer cells.^[38] Being
10 metastasis the primary cause of death for most cancers, we believe these new property of
11 MWCNTs position these nanomaterials as a new ground-breaking type of future synthetic
12 microtubule-stabilizing therapies that could play a pivotal role in future cancer treatment.
13
14
15
16
17
18
19
20
21
22
23
24
25
26
27
28
29
30
31
32
33
34
35
36
37
38
39
40
41
42
43
44
45
46
47
48
49
50
51
52
53
54
55
56
57
58
59
60
61
62
63
64
65

Experimental Section

MWCNTs synthesis and characterization

CNTs of 3 to 12 walls, with outer diameter ranging from 5 to 15 nm were synthesized following the catalytic chemical vapor deposition method using Co and Mo particles as catalyst.^[39] An aqueous HCl treatment procedure was applied to clean and separate the MWCNTs from contaminants. The *as-prepared* MWCNTs were characterized by various techniques including Raman spectroscopy, transmission electron microscopy (TEM) and thermo-gravimetric analyses (TGA) (**Supporting Figure 2**). MWCNTs produce a characteristic Raman spectrum distinguishable of SWCNTs spectrum revealing typical MWCNT resonances^[40] such as the dispersive disorder induced D band at 1330 cm⁻¹, the tangential G band at 1586 cm⁻¹ and the D' band at 1614 cm⁻¹. TEM was performed in a JEOL JEM 2100 microscope operating at 120 kV. Samples were prepared using ethanol as dispersant and omitting the sample centrifugation steps. A drop of this suspension was adsorbed onto a Lacey copper grid. The TGA was performed with a Perkin Elmer Pyris 1 system. Measurements were conducted by heating 9-12 mg of MWCNTs in dry air from 35° C up to 1000° C at a rate of 2° C min⁻¹. TGA results showed a typical characteristic CNT curve where the oxidations of hexagonal carbon ring appeared at 550° C. Qualitative information on the purity of CNT could be obtained from the TGA based on the extent of non-oxidizable residues at high temperature. In our measurements, catalytic metal impurities were not observed between 600 and 1000° C. All these techniques confirmed the absence of undesired impurities in these MWCNTs samples.

MWCNTs dispersion and functionalization

CNTs were de-bundled and dispersed by repeated cycles of vortex mixing followed by mild sonication (3 min, frequency of 20 kHz, 130 W in a SONICS Vibracell VCX130) and

centrifugation in cell culture medium (DMEM, Dulbecco's Modified Eagle Medium from SIGMA-ALDRICH) containing serum and antibiotics as previously described.^[10-13] The stability of the stock suspension was checked by centrifugation at 14.000 g after each sonication cycle. Visible absorption was used to determine MWCNT concentration in the 400-600 nm range. Further details of the stability and dispersion of MWCNTs in the cell culture medium can be found in previous work.^[10,11] A total of 3-5 cycles were sufficient to obtain a well-dispersed concentrated suspension of MWCNTs which was re-diluted in culture medium to the concentrations indicated in the text.

Confocal Raman Spectroscopy Imaging

A confocal Raman microscope (Alpha300, WITec) equipped with a piezo scanner and a linear polarized frequency doubled Nd:YAG laser (532 nm excitation wavelength) focused through an air objective (Nikon, 100X, NA= 0.9) was used. To avoid damage and heating, the laser power was controlled below 2 mW. The spatial resolution is diffraction limited. In the set-up used, features at a distance of $r = 0.61 \times 532/0.9 = 0.36 \mu\text{m}$ can be distinguished and completely resolved at a distance of $0.72 \mu\text{m}$. Mapping was done for the stack scan with a step size of $0.36 \mu\text{m}$ in X/Y and a constant Z (depth) in a square of $23 \mu\text{m} \times 25 \mu\text{m}$ on X/Y. To get a better signal-to-noise ratio, every spectrum was acquired with an integration time of 0.3 s, meaning $75 \times 75 = 5625$ spectra for one image. Images from this multi-spectra file were computed by integrating the appropriate Raman peaks using the ScanCtrlSpectroscopyPlus software (WITec, Germany). The images were constructed mapping the signals of G mode ($1500\text{-}1700 \text{ cm}^{-1}$) and the C-H stretching in the $2800\text{-}3000 \text{ cm}^{-1}$ region.^[41]

Cell culture, cell tracking and imaging techniques

The human cancer cell line models used (HeLa, MCF7, SH-SY5Y and U87MG) have been thoroughly characterized in the literature.^[42-44] Primary GBM cell cultures have been

previously characterized by our group.^[25] Cells were grown in DMEM media containing 10 % FCS at 37°C, 5 % CO₂ and were exposed to 25 µg/ml MWCNTs concentration in the culture medium for 70 h (unless otherwise indicated). Controls and MWCNT-treated cells were grown on the same culture plate and were imaged simultaneously. Centrosomal trajectories were labelled by gene-transfer with a vector expressing GFP:EB1 in HeLa cells 24 h before exposure to MWCNTs in the medium. This vector was kindly provided by Dr. Akhmanova (Utrecht University, The Netherlands). Nuclear DNA was labelled with Hoechst dye (Bis-benzimide) (Sigma-Aldrich). Cell tracking analysis was performed on *time-lapse* video microscopy movies obtained @ 15 min/frame during 5 h on a Nikon Eclipse Ti live-cell station, using a 10X Nikon N.A. 0.45. Quantification analysis was performed with the NIS-Elements software. The average cell migration speed was obtained for a minimum of hundred cells in at least 3 sets of experiments for each condition. Actual numbers of analyzed cells are designated in Table 1 as degrees of freedom (*DF*). Unpaired two-tailed Student's *t* test was used for the statistical evaluation of differences between control and treated cells. Probability (*p*) values are also shown.

Supporting Information

Supporting Information is available from the Wiley Online Library or from the author.

Acknowledgements

We are very grateful L. Alvarez-Montes and to J. Díaz-Gómez for their help and to the Nikon A1R Laser Microscopy Unit of the IDIVAL Institute. We also thank Dr. Baylo and Dr. Toporski of the WITec Company for their help with the confocal Raman imaging. This work has been supported by the Spanish ISCIII-MINECO under Projects ref. PI13/01074, AES 2013; MAT2012-38664-C02-01; MALTA Consolider-Ingenio ref. CSD2007-00045, PI10/02002, AES 2010, and the Spanish ISCIII programs RTICC refs. RD06/0020/0074 and RD12/0036/0022. We especially thank Fundación Eugenio Rodríguez Pascual (“ayudas de investigación” 2014, ref. 02-H048-64003) to MLF.

Received: ((will be filled in by the editorial staff))

Revised: ((will be filled in by the editorial staff))

Published online: ((will be filled in by the editorial staff))

References

- [1] S. Park, D. Srivastava, K. Cho, *NanoLett.* **2003**, 3, 1273-1277.
- [2] X. Shi, A. Von demBussche, R.H. Hurt, A. B. Kane, H. Gao, *Nat Nanotechnol* **2011**, 6, 714–719.
- [3] L. Lacerda, J. Russier, G. Pastorin, M. A. Herrero, E. Venturelli, H. Dumortier, K. T. Al-Jamal, M. Prato, K. Kostarelos, A. Bianco, *Biomaterials* **2012**, 33, 3334–3343.
- [4] E. Mooney, P. Dockery, U. Greiser, M. Murphy, V. Barron, *Nano Lett.* **2008**, 8, 2137-2143.
- [5] L. M. Sargent, A. F. Hubbs, S. H. Young, M. L. Kashon, C. Z. Dinu, J. L. Salisbury, S. A. Benkovic, D. T. Lowry, A. R. Murray, E. R. Kisin, K. J. Siegrist, L. Battelli, J. Mastovich, J. L. Sturgeon, K. L. Bunker, A. A. Shvedova, S. H. Reynolds, *Mutat. Res. - Genet. Toxicol. Environ. Mutagen.* **2012**, 745, 28-37.
- [6] A. E. Porter, M. Gass, K. Muller, J. K. Skepper, P. A. Midgley, M. Welland, *Nat. Nanotechnol.* **2007**, 2, 713-177.
- [7] H. Ali-Boucetta, A. Nunes, R. Sainz, M. A. Herrero, B. Tian, M. Prato, A. Bianco, K. Kostarelos, *Angew. Chem. Int. Ed. Engl.* **2013**, 52, 2274-2278.
- [8] X. Li, Y. Peng, X. Qu, *Nucleic Acids Res.* **2006**, 34, 3670–3676.
- [9] H. Shams, B. D. Holt, S. H. Mahboobi, Z. Jahed, M. F. Islam, K. N. Dahl, M. R. Mofrad. *ACS Nano.* **2014** 8, 188-197.
- [10] J. C. Villegas, L. Álvarez-Montes, L. Rodríguez-Fernández, J. González, R. Valiente, M. L. Fanarraga, *Adv Healthc Mater* **2014**, 3, 424-432.
- [11] L. Rodríguez-Fernández, R. Valiente, J. González, J. C. Villegas, M. L. Fanarraga, *ACS Nano* **2012**, 6, 6614-6625.
- [12] F. Pampaloni, E. L. Florin, *Trends Biotechnol.* **2008**, 26, 302–310.
- [13] C. Z. Dinu, S.S. Bale, G. Zhu, J.S. Dordick, *Small* **2009**, 5 310-315.

- [14] E. Nogales, M. Whittaker, R. A. Milligan, K. H. Downing. *Cell* **1999**, 96, 79-88
- [16] T. Mitchison, M. Kirschner, *Nature* **1984**, 312, 237-42.
- [17] M. A. Jordan, L. Wilson, *Curr Opin Cell Biol.* **1998**, 1, 123-130.
- [18] D. R. Matson, P. T. Stukenberg, *Mol. Interv* **2011**, 11, 141-150.
- [19] J. Zhou, P. Giannakakou, *Curr. Med. Chem. Anti-Cancer Agents* **2005**, 5, 65-71.
- [20] L. Gonzalez, I. Decordier, M. Kirsch-Volders, *Biochem. Soc. Trans.* **2010**, 38, 1691–1697.
- [21] G. W. Luxton, G. G. Gundersen, *Curr. Opin. Cell. Biol.* **2011**, 23, 579-588.
- [22] E. Van Beneden, *Arch. Biol.* **1883**, 4, 265–638.
- [23] R. Li, G. G. Gundersen, *Nat. Rev. Mol. Cell. Biol.* **2008**, 9, 860-873.
- [24] A. Bédier, F. Seichepine, E. Flahaut, I. Loubinoux, L. Vaysse, C. Vieu. *Langmuir* 2012 Dec 18;28(50):17363-71. *Langmuir* **2012** 28, 17363-17371.
- [25] P. Ruiz-Ontañón, J. L. Orgaz, B. Aldaz, A. Elosegui-Artola, J. Martino, Berciano M. T, J. A. Montero, L. Grande, L. Nogueira, S. Diaz-Moralli, A. Esparís-Ogando, A. Vazquez-Barquero, M. Lafarga, A. Pandiella, M. Cascante, V. Segura, J. A. Martinez-Climent, V. Sanz-Moreno, J. L. Fernandez-Luna, *Stem Cells* **2013**, 31, 1075-1085.
- [26] M. J. O'Connell, SM. Bachilo, C. B. Huffman, V. C. Moore, M. S. Strano, E. H. Haroz, K L. Rialon, P. J. Boul, W. H. Noon, C. Kittrell, J. Ma, R. H. Hauge, R. B. Weisman, R. E. Smalley, *Science* **2002**, 297, 593–596.
- [27] D. A. Heller, P W. Barone, J. P. Swanson, R. M. Mayrhofer, M. S. Strano, *J. Phys. Chem. B* **2004**, 108, 6905–6909.
- [28] M. S. Strano, C. B. Huffman, V. C. Moore, M. J. O'Connell, E. H. Haroz, J. Hubbard , M. Miller, K. Rialon, C. Kittrell, S. Ramesh, R. H. Hauge, R. E. Smalley, *J. Phys. Chem. B* **2003**, 107, 6979–6985.

- [29] E. Joselevich, H. Dai, J. Liu, K. Hata, A. H. Windle. *Topics Appl. Physics* Vol. 111 (Eds: A. Jorio, D. S. Dresselhaus, G. Dresselhaus), Springer-Verlag, Germany **2008**, *Carbon Nanotubes*,
- [30] S. F. Chin, R. H. Baughman, A. B. Dalton, G. R. Dieckmann, R. K. Draper, C. Mikoryak, I. H. Musselman, V. Z. Poenitzsch, H. Xie, P. Pantano, *Exp. Biol. Med.* **2007**, 232, 1236–1244.
- [31] M. S. Arnold, M. O. Guler, M. C. Hersam, S. I. Stupp, *Langmuir* **2005**, 21, 4705–4709.
- [32] G. R. Dieckmann, A. B. Dalton, P. A. Johnson, J. Razal, J. Chen, GM. Giordano, E. Muñoz, I. H. Musselman, R. H. Baughman, R. K. Draper, *J. Am. Chem. Soc.* **2003**, 125, 1770–1777.
- [33] S. S. Karajanagi, H. C. Yang, P. Asuri, E. Sellitto, J. S. Dordick, RS. Kane, *Langmuir* **2006**, 22, 1392–1395.
- [34] W. J. Huang, S. Taylor, K. Fu, Y. Lin, D. Zhang, T. W. Hanks, A. M. Rao, Y. P. Sun. *NanoLett.* **2002**, 2, 311–314.
- [35] C. Y. Tay, M. I. Setyawati, J. Xie, J. W. Parak, D. T. Leong. *Adv. Fuc. Mat.* **2014** 24, 5936-5955.
- [36] C. Y. Tay, P. Cai, M. I. Setyawati, W. Fang, L. P. Tan, C. H. Hong, X. Chen, D. T. Leong. *Nano Lett.* **2014** 14, 83-8.
- [37] L. García Hevia, F. Fernández, C. Grávalos, A. García, J. C. Villegas, M. L. Fanarraga, *Nanomedicine* **2014**, 9, 1581-1588.
- [38] G. A. Orr, P. Verdier-Pinard, H. McDaid, S. B. Horwitz, *Oncogene* **2003**, 22, 7280–7295.
- [39] E. Flahaut, C. H. Laurent, A. Peigney, *Carbon* **2005**, 43, 375–383.
- [40] S. Dresselhaus, G. Dresselhaus, R. Saito, A. Jorio, *Phys. Rep.* **2005**, 409, 47–99.
- [41] P. R. Griffiths, E. V. Miseso, *Infrared and Raman instrumentation for mapping and imaging*, (Eds: R. Salzer, HW. Siesler), Wiley-VCH, Weinheim, Germany. **2009**, 1–64

- [42] H. D. Soule, J. Vazquez, A. Long, S. Albert, M. Brennan, *Natl. Cancer. Inst.* **1973**, 51, 1409-1416.
- [43] H. R. Xie, L. S. Hu, G. Y. Li, *Chin. Med. J. (Engl.)* **2010**, 123, 1086-1092.
- [44] M. J. Clark, N. Homer, B. D. O'Connor, Z. Chen, A. Eskin, H. Lee, B. Merriman, S. F. Nelson, *PLoS Genet.* **2010**, 6, e1000832.

Tables:

Table 1. Migration inhibitory effect of MWCNTs for different cancer cells types

Cell type	Control speed ^{a)}	MWCNT speed ^{a)}	Speed reduction	DF ^{b)}	<i>t/p</i> ^{c)}	% Statistical Significance
HeLa	12.7 ± 0.6	7.4 ± 0.4	41 %	245	7.2/ <10 ⁻¹⁰	>99.99
MCF7	1.6 ± 0.1	1.5 ± 0.1	6 %	130	0.4/ 0.64	NS
SH-SY5Y	8.7 ± 0.7	6.8 ± 0.4	22 %	114	2.3/ 0.02	95-98
U87MG	8.5 ± 0.2	6.1 ± 0.2	28 %	249	7.1/ <10 ⁻¹⁰	>99.99
GBM	9.2 ± 0.2	7.5 ± 0.1	18.5 %	408	6.5/ <10 ⁻⁹	>99.99

^{a)} Average speeds is shown in nm/s; ^{b)} DF= Degrees of Freedom; ^{c)} *t/p* = student's *t* test and *p* probability.

Figures:

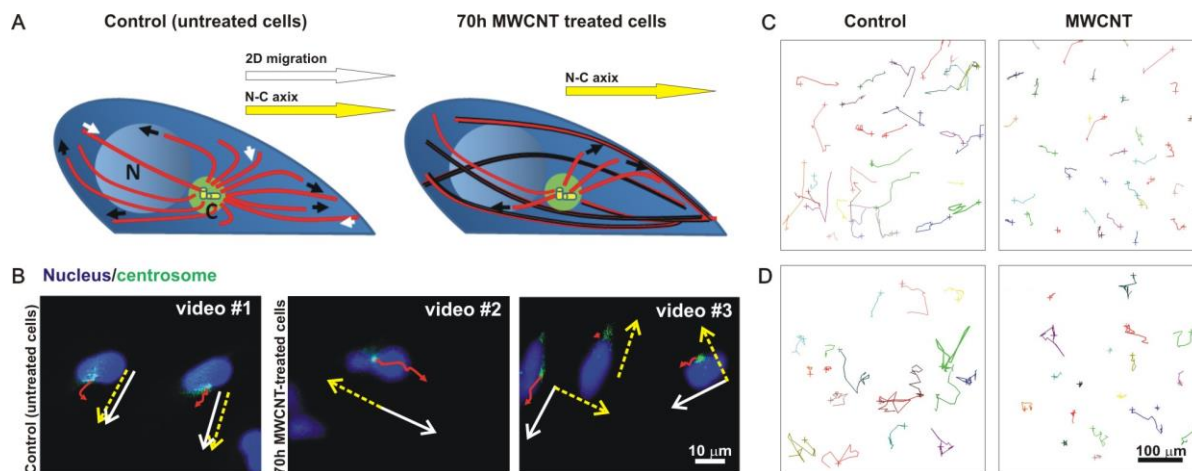


Figure 1. MWCNTs produce centrosomal miss-positioning and disrupt the nuclear-centrosomal axis hindering cell migration.

A) Diagram of the disposition of the nucleus (N), centrosome (C, green) and microtubule array (red filaments) in control and MWCNT-treated (MWCNTs in black) migrating cells. Microtubule traction forces are also represented (small white and black arrows). The cell polarity and migratory direction (white arrow) relative to the nuclear-centrosomal axis (yellow arrow) is indicated.

B) Frozen live-cell images obtained from *time-lapse* videos 1-3 (**Supporting Video 1-3**) of migrating HeLa cells displaying labelled nuclei (blue) and centrosomes (green). The centrosomal trajectories (red arrows), average cell trajectories (white arrows) and nuclear-centrosomal axes (yellow arrows) are shown for MWCNT-treated cells and untreated controls.

C-D) Representative glioblastoma (U87MG) and neuroblastoma (SH-SY5Y) 5 h cell tracking trajectories, respectively. Cultures grown in the absence (control) or presence of MWCNTs were recorded during 70 h. Individual cell trajectories indicated by colored lines, are shorter in cells incubated with MWCNTs.

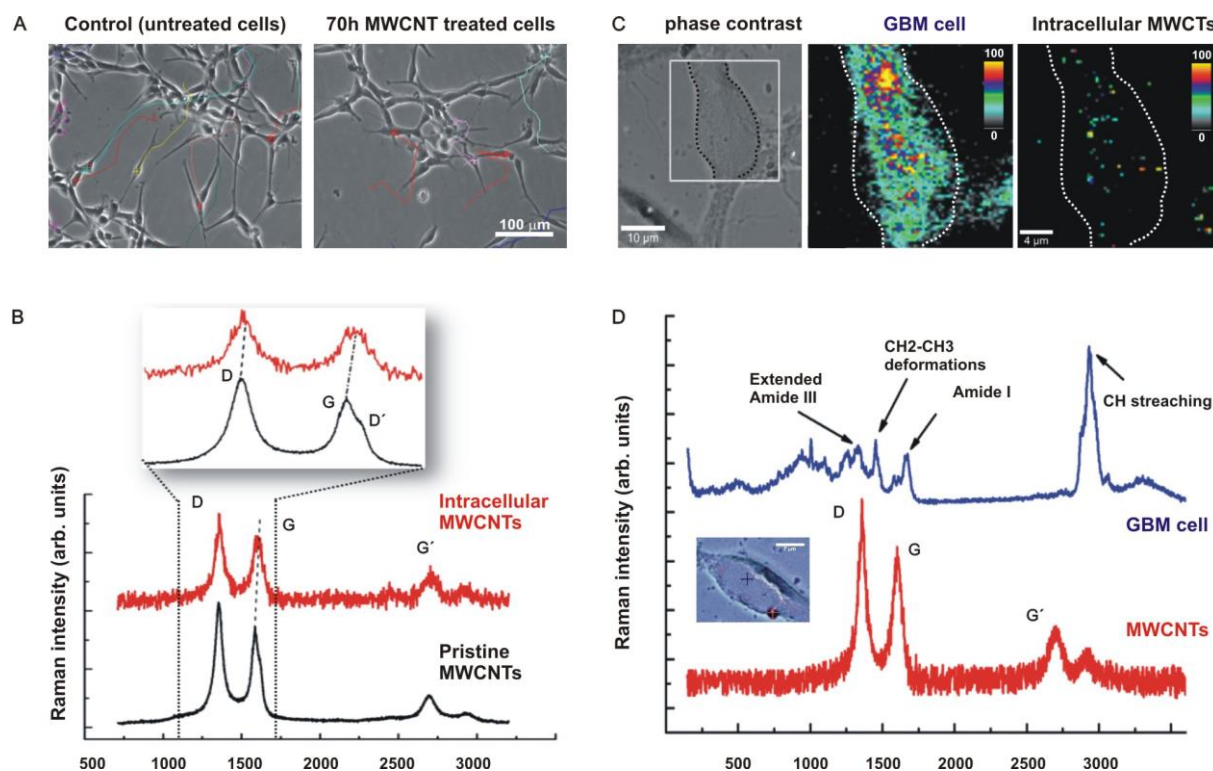


Figure 2. MWCNTs translocate into the cytoplasm of surgical specimen-derived cancer cells and interfere with cell spreading.

A) Phase contrast microscopy images of the primary cultures of GBM cells obtained from surgical specimens. Both control and MWCNT-treated cells display a long bipolar morphology and no observable toxicity signs. Colored lines indicate 5 h cell trajectories.

B) Comparison between the Raman spectra of pristine MWCNTs (black) and intracellular MWCNTs (red trace). These Raman spectra were obtained with a 532 nm line of a linear polarized frequency doubled Nd:YAG laser. The inset shows a detail of the typical fingerprints expected for MWCNTs spectral region corresponding to the D and G bands in order to point out the blue-shift of the Raman peak frequencies associated with the functionalization of the intracellular MWCNTs. Though only minor differences in the peak positions are observed, the spectrum of MWCNTs treated glioblastoma cell is slightly shifted

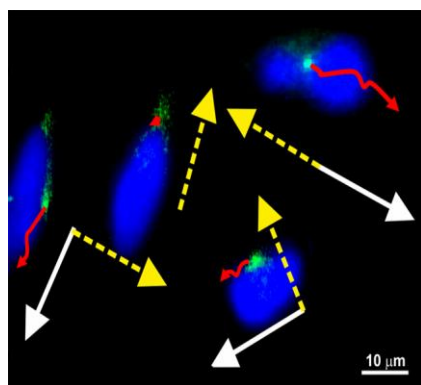
to higher wavenumbers and a decrease in Raman intensities of D and, G and G' modes are observed (**Supporting Table 1**).

C) Phase contrast image a GBM cell captured through 100X objective of the confocal Raman microscope. (center) Single confocal Z plane Raman image of the same cell obtained integrating the intensities in the 2800-3000 cm^{-1} region (C-H stretching), integration time of 0.3 s x 10 accumulations and a point spacing of 0.36 μm . (right) Confocal Raman image obtained at the same confocal Z plane to determine the localization of intracellular MWCNTs integrating the Raman intensities of the G-band (1500-1700 cm^{-1} region). As shown in the color scale (indicating maximum/minimum CCD counts), bright yellow hues indicate the highest signals and grey hues low integrated G band intensities.

D) Confocal Raman spectra of the cytoplasm of a MWCNT-treated GBM cell (inset, blue cross) and extracellular functionalized MWCNTs (inset, red cross). Integration time of 0.5 s x 10 accumulations and 0.3 s x 10 accumulations, respectively.

The table of contents:**Inhibiting cancer cell migration and infiltration to other tissues makes the difference**

between life and death. MWCNTs display intrinsic biomimetic properties with microtubules, severely interfering with the function of these filaments during cell proliferation, triggering cell death. Here we demonstrate how MWCNTs disrupt the centrosomal microtubule cytoskeletal organization in cancer cells triggering potent anti-migratory effects. Our data validate these nanomaterials as future adjuvant therapies to boost the effect of traditional microtubule-stabilizing anti-cancer drugs.

**Keywords:**

- Cytoskeleton,
- tubulin polymers,
- biomechanics,
- cancer,
- metastasis.

Title: Inhibition of Cancer Cell Migration by Multiwalled Carbon Nanotubes